ELSEVIER

Solar Energy Materials & Solar Cells 72 (2002) 59–68

Solar Energy Materials & Solar Cells

www.elsevier.com/locate/solmat

Numerical simulations for silicon crystallization processes—examples from ingot and ribbon casting

I. Steinbach*, M. Apel, T. Rettelbach, D. Franke

ACCESS e.V., Intzestr. 5, 52072 Aachen, Germany

Abstract

At ACCESS e.V. numerical simulations of casting and heat treatment processes are performed and are in use for process optimization since more than 10 years. During the last few years, a simulation technique, for the prediction of microscale texture characteristics dependent on the solidification conditions, has been additionally developed. Both simulation methods are applied to silicon crystallization processes in close collaboration with partners from the industry, namely the Deutsche Solar GmbH.

In this paper, general features of numerical simulation for silicon crystallization techniques will be presented. The prospectives and limitations of these simulation methods will be discussed. Finally, examples of numerical simulation results on different length scales for two silicon-casting processes are given.

Keywords: Multicrystalline silicon; Crystallization; Numerical simulation

1. Introduction

Numerical simulation has emerged in the last decade as an effective tool in development and optimization of technical processes. This is especially true for processes with high demand on quality and high added value to the product. Because of extreme demands on quality and having an added value of more than a factor of 10 from feedstock to the sliced wafer, single-crystal pulling of silicon has been investigated by numerical simulation since the early days of numerical simulations (see, e.g. Ref. [1]). Specially tailored numerical tools were applied to investigate the

*Corresponding author. Tel.: +49-241-8098012; fax: +49-241-38578.
E-mail address: i.steinbach@access.rwth-aachen.de (I. Steinbach).

0927-0248/02/$ - see front matter
PII: S0927-0248(01)00150-7

crystallization conditions in the puller, starting from simple approximations of heat fluxes and steadily growing to complex systems addressing radiative heating, melt flow including electromagnetic stirring, argon flow, segregation of impurities, oxygen and carbon including thermodynamic equilibrium at the phase boundaries.

Due to the highly specialized nature of the applications, however, the transfer of the models to ingot casting of multicrystalline silicon or furthermore to silicon ribbon casting is difficult. Additionally, the ingot casting and crystallization in the power down process or Bridgman process is of transient nature when compared to the more or less steady state process of crystal pulling, and approximations of rotational symmetry are no longer applicable.

In this paper, the principles of the processes of crystal pulling, ingot casting and ribbon casting are shortly reviewed with respect to the consequences for the theoretical models of the process. Then, the numerical approach used at ACCESS is described and examples of process simulations are given.

2. Principles of crystallization from the melt

From a mathematical point of view, crystallization of silicon can be described as a moving-boundary problem, where the crystallization front defines the moving boundary between the crystal and the liquid. The set of equations is

$$\rho c_p \frac{\partial T}{\partial n} = \lambda \nabla^2 T, \tag{1}$$

$$\lambda \left.\frac{\mathrm{d}T}{\mathrm{d}n}\right|_{\mathrm{m}} - \lambda \left.\frac{\mathrm{d}T}{\mathrm{d}n}\right|_{\mathrm{c}} = L v_{\mathrm{c}}, \tag{2}$$

$$T|_{\mathrm{m/c}} = T_{\mathrm{c}},$$

ρc_p: specific heat (J/cm^3 K)
T: temperature (K)
T_{c}: crystallization temperature (K)
λ: heat conductivity (W/cm K)
d/dn: derivative in normal direction to the crystallization front (1/cm)
L: latent heat of crystallization (J/cm^3)
v_{c}: velocity of crystallization (cm/s)

Eq. (1) is the heat transport equation that has to be solved in both crystal and melt phases including convective heat transport in the melt. Eq. (2) is the so-called Stephan condition connecting the heat flow at the melt side (index m) and the crystal side (index c) of the crystallization front to the release of latent heat during crystallization with velocity v_{c}. In crystals with strong covalent binding and high melting point, like silicon, the latent heat is extraordinarily high (approx. 3300 J/cm^3). For a typical crystallization velocity of 2 cm/h, a heat flux of approximately 2 W/cm^2 is needed corresponding to a thermal gradient in the crystal

which is greater than 20 K/cm. The temperature profile perpendicular to the crystallization front is depicted in Fig. 1. The sharp kink of the temperature profile at the position of the crystallization front is the result of the latent heat release. The control of the crystallization is then possible by controlling the heat fluxes on both sides of the front.

In general, there are two different strategies of this control for the Czochralsky crystal pulling (Cz) and ingot casting. Fig. 2 explains the schematics of the processes. In both cases, the dominant heat flux is the heat extraction through the crystal (upside in Cz, downside in the ingot process).

The general strategy in Cz is to reach steady state heat flow by cooling the crystal over its sides. This allows for the pulling of long single crystals (up to 2 m in technical processes).

The drawback of this strategy is the strong radial heat flux, which causes an upward bent crystallization front and high elastic stress in the solid.

The strategy of the ingot casting process is to control the temperatures at the outside of the casting crucible and on top of the melt in order to control the crystallization. In modern processes with planar crystallization front (e.g. SOPLIN [2]), this allows for a nearly unidirectional heat flow through the bottom of the casting, avoiding high thermal stresses and thus reducing the dislocation density of the multicrystalline material.

The disadvantage of this strategy is that the temperatures have to be controlled in such a manner that the growing heat resistivity of the growing crystal is compensated. As the exact position of the crystallization front is difficult to detect in the ingot casting process, an optimal control has to be based on indirect measurements or by means of numerical process simulation.

Other crystallization processes like continuous casting or ribbon growth in vertical direction may be related to the Cz process while ribbon growth in horizontal direction (RGS) may be related to the ingot casting process.

The numerical models applied to simulate the different crystallization processes now reflect the different strategies of process control: To simulate the Cz process

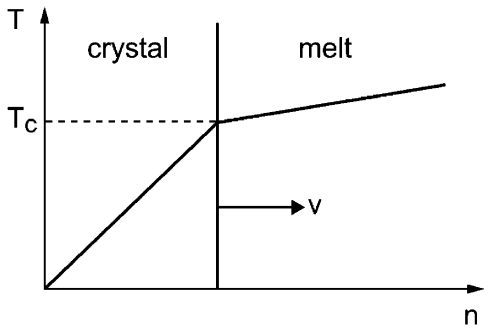

Fig. 1. Scheme of the temperature profile in normal direction through the crystallization front, which moves with velocity v.

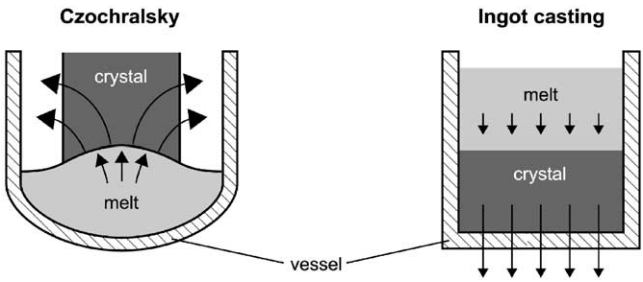

Fig. 2. Scheme of the Cz and ingot casting process. The dominant heat flux is through the crystal.

with its quasi-steady state conditions, it is common to adapt the numerical grid to the solid respectively liquid part of the silicon. The grid is considered quasi-stationary and the release of latent heat of crystallization is realized as a boundary condition between the crystal and the melt. The movement of the solid is either neglected or incorporated by making an advective contribution to the heat conduction equation. This approach allows for a sharp description of the temperature profile at the crystallization front. Further on, often rotational symmetry can be assumed which drastically improves the computational efficiency compared to a full three-dimensional (3D) calculation.

For the ingot process, the assumption of quasi-steady state condition is not valid. Therefore, the full moving-boundary problem of crystallization has to be solved. The method of choice is the enthalpy method, where the latent heat of crystallization is smeared out over a certain temperature interval ΔT_c around the melting temperature (see Fig. 3): One finite element or control volume, that is intersected by the crystallization front now has to lie in the temperature range ΔT_c. It may be attributed to a fraction of crystal f_c, the volume fraction of the crystalline state inside the element or volume that is related to its temperature by the enthalpy function $E(T)$.

$$f_c = \begin{cases} 1, & T < T_c - \dfrac{\Delta T}{2}, \\ \dfrac{E(T_c + \Delta T/2) - E(T)}{L}, & T_c - \dfrac{\Delta T}{2} < T < T_c + \dfrac{\Delta T}{2}, \\ 0, & T > T_c + \dfrac{\Delta T}{2}. \end{cases} \tag{3}$$

As T_c varies in this formulation continuously from 0 to 1, the velocity of the crystallization front can be written as follows:

$$v = \frac{dn}{dt} = \frac{dn}{df_c}\frac{df_c}{dt} = \left(\frac{df_c}{dn}\right)^{-1} \dot{f}_c, \tag{4}$$

where n is the normal coordinate of the crystallization front.

Inserting Eq. (4) into the Stephan condition (2) and evaluating $\nabla^2 T$ in the smeared out phase boundary, the whole problem can be reformulated into one

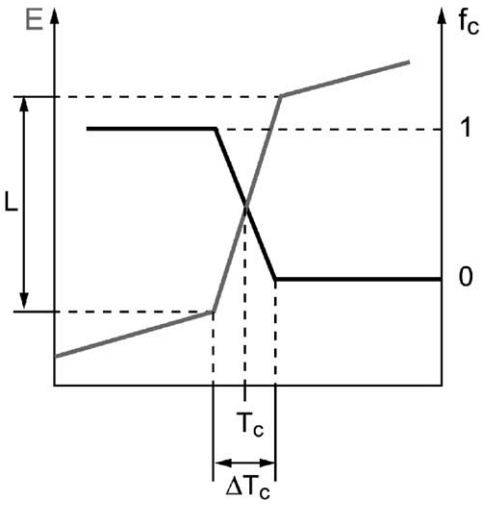

Fig. 3. Scheme of the relation between enthalpy as a function of temperature and the local fraction of crystal.

equation

$$\rho c_p \frac{\partial T}{\partial T} = \lambda \nabla^2 T + L \dot{f}_c, \tag{5}$$

where the last term accounts for the release of latent heat. Using

$$\dot{f}_c = \frac{\mathrm{d}f_c}{\mathrm{d}T}\dot{t}, \tag{6}$$

we end with the simple equation

$$\left(\rho c_p - L\frac{\partial f_c}{\mathrm{d}T}\right)\dot{T} = \lambda \nabla^2 T \tag{7}$$

which can be solved almost fully implicitly. The artificial interval of crystallization ΔT_c finally can be adjusted according to

$$\Delta T_c = \nabla T \cdot \Delta x, \tag{8}$$

where ∇T is the average temperature gradient at the crystallization front and Δx the average grid spacing.

On the microscopic length scale, the condition of local equilibrium, expressed by the fixed relation between f_c and E in Eq. (3), is no longer valid. Then, the fraction of crystal f_c becomes an independent degree of freedom. $f_c \to \phi(x)$, the so-called phase field parameter, that describes the local phase state. This degree of freedom has to be treated with its own dynamics according to the supercooling of the crystallization front. Details of this microscopic model are described elsewhere [3].

3. Examples

Ingot casting for the production of multicrystalline silicon for solar cells was established by Wacker with the so-called SilSo process [5]. From its principles, this process is highly transient due to the fast heat extraction into the crucible after the casting and the slow end of crystallization. In order to overcome these disadvantages, more elaborate casting strategies have been investigated. Fig. 4 shows a late stage of the process development [6]. The crucible is covered at the sides by a thick layer of insulation to reduce radial heat flow. One top heater was available to control the crystallization. The planarity of the crystallization front was greatly improved by the insulation, but still showed pronounced curvature in the corners of the ingot (see Fig. 4).

In Fig. 5, the calculated temperature history throughout the casting process beginning with preheating of the crucible over the transport of the crucible to the casting position, casting, crystallization and to the cooling is shown. Position 2 shows the temperature at the position of a pyrometer hole in the insulation that was used for process control. Significant features are sharp temperature drops during transport. During crystallization, the segregation of iron was calculated on the basis of the local crystallization velocity (Fig. 6a and b). The velocity decreases from its maximum value of 2.5×10^{-5} to roughly 0.2×10^{-5} cm/s. Correspondingly, the segregation changed its pattern from diffusive-controlled segregation to convective-controlled segregation. This results in a maximum iron concentration at approx. 5 cm height in the ingot. This calculated effect correlated well with an experimentally observed minimum in carrier lifetime at this position. Fig. 7 shows a corresponding simulation of the SOPLIN process. In this example, the necessity of experimental verification and calibration of the numerical simulations shall be highlighted. The actual process control is mirrored nicely in the kinks of the time–temperature plots. These kinks mark the actual position of the solidification front as well as the change

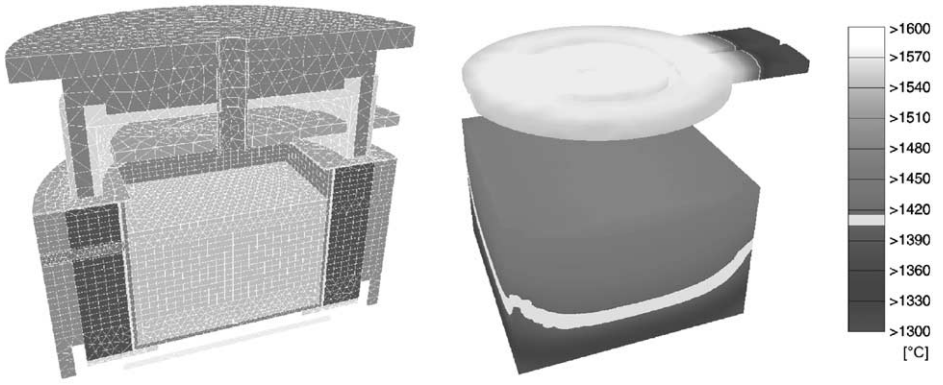

Fig. 4. Calculation of temperature distribution during crystallization in the cold wall process of Wacker. The bright line indicates the crystallization front. Left: FE geometry of the growth chamber.

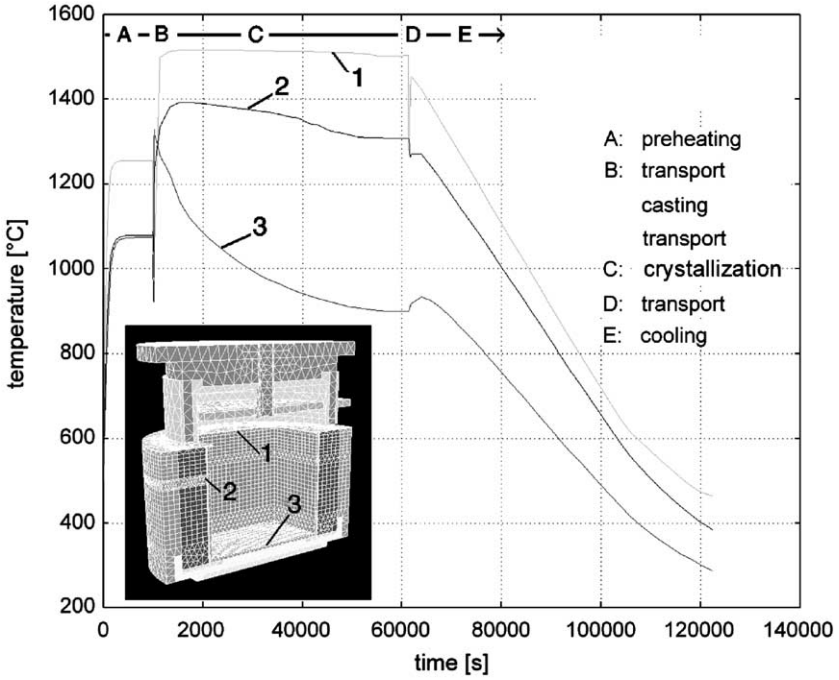

Fig. 5. Calculated temperature during the whole process cycle from preheating of the vessel to cooling of the ingot. The inset indicates the position where the temperatures are evaluated.

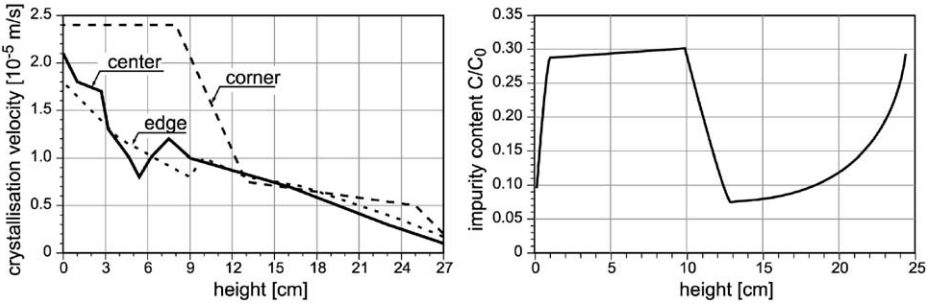

Fig. 6. Calculated solidification velocities (a) and corresponding impurity concentration (b) relative to mean impurity concentration c_0 over the height of the ingot.

in heater control. Process optimization and control of dislocation multiplication by the use of numerical simulation is described elsewhere [4].

The application of numerical simulation to the development of the RGS-silicon ribbon growth process is given in Fig. 8. The process modelling was focused on the optimal design of casting frame and the heaters (not shown in Fig. 8) and on the

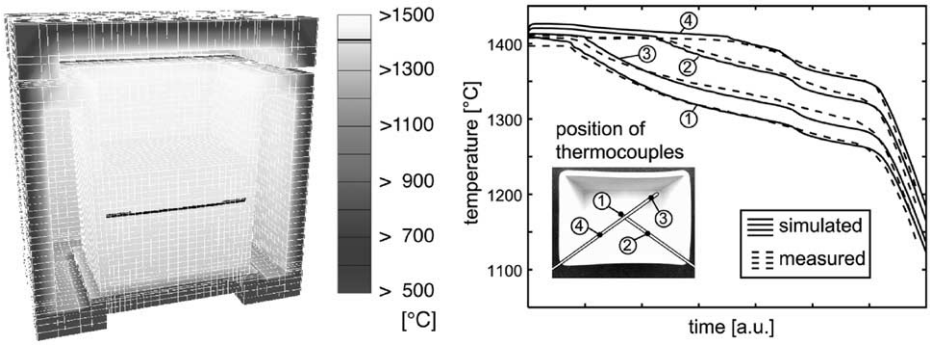

Fig. 7. Calculated temperature distribution in the SOPLIN process. The crystallization front is indicated by the dark line. The time–temperature profiles give the correlation between the calculation and experiment.

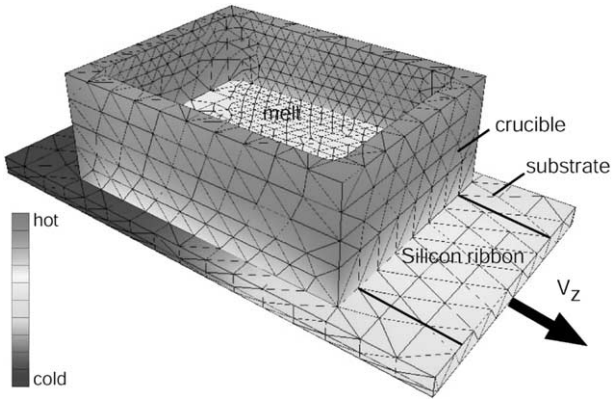

Fig. 8. Calculation of the temperature distribution in the casting frame of the RGS process.

thermal interaction of the silicon and the moving substrate. For this problem, a further step to microscopic modelling of crystallization was taken. Fig. 9 shows two situations of the growth of the tip of the crystallization front—the very start of crystallization—into the supercooled silicon melt on the cold substrate [3,7]. Depending on the process conditions, dendritic crystallization with long needle-like crystals, or columnar globulitic growth can be expected, as proven by the characterization of RGS-ribbons. Details and application of this simulation technique are presented in [7]. As a last example and as an outlook, the microscopic simulation of grain selection during the ingot casting process is given (Fig. 10). Here, the faceted anisotropy of the crystal surface plays an important role. This type of simulation shows at present realistic features of the real process. Due to the complexity of the underlying physics, it is, however, still far from being used in practical applications.

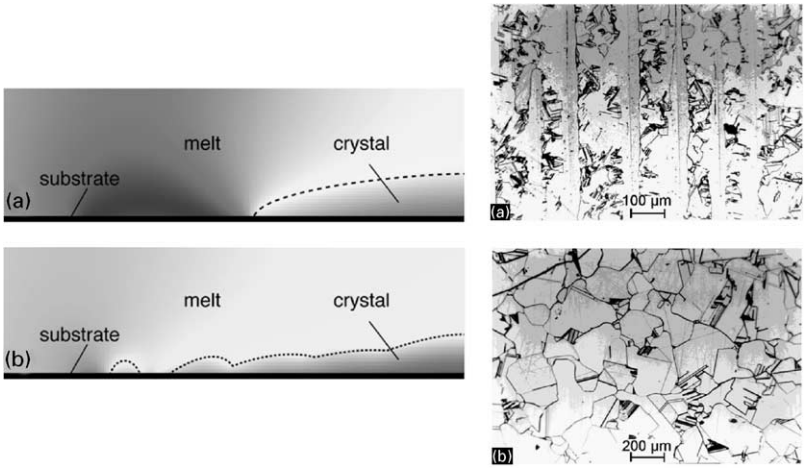

Fig. 9. Calculated temperature at the tip of the crystallization front in the RGS process for stable dendritic growth (a) and columnar globulitic growth (b). The experimentally produced grain structures correspond to these predictions.

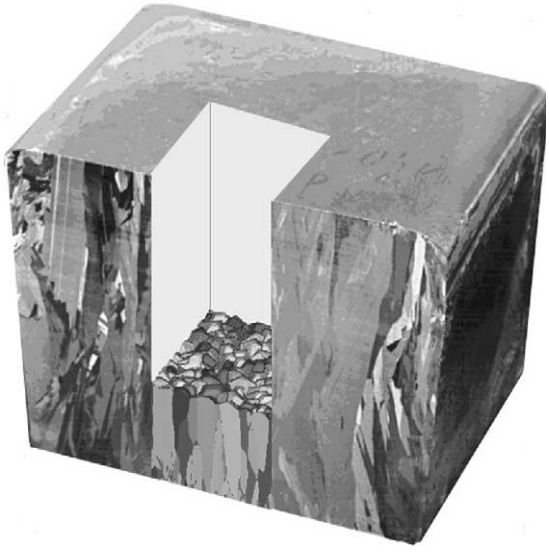

Fig. 10. Grain structure on the half-cut of a cast ingot from the SOPLIN process. In the center of the ingot a calculated grain structure is shown.

4. Conclusion

The principles of the heat flow problem during crystallization are briefly reviewed. As a consequence of the different control strategies in Cz and ingot growth

processes, different numerical schemes are applied for the simulation of these processes. The transient nature of the ingot casting process is best resolved by the enthalpy scheme of solidification.

Examples of simulations of ingot casting and ribbon casting are presented on the macroscopic level of process control and the microscopic level of crystallization.

References

[1] C.J. Chang, R.A. Brown, J. Crystal Growth 63 (1983) 343.
[2] W. Koch, W. Krumbe, I.A. Schwirtlich, Proceedings of the 11th European Conference on Photovoltaic Solar Energy Conversion, Montreux, 1992, p. 518.
[3] M. Apel, D. Franke, I. Steinbach, Simulation of the crystallization of silicon ribbons on substrate, Sol. Energy Mater. & Sol. Cells, (2002), this issue.
[4] D. Franke, T. Rettelbach, C. Häßler, W. Koch, A. Müller, Silicon ingot casting: process development by numerical simulations, Sol. Energy Mater & Sol. Cells, (2002), this issue.
[5] D. Helmreich, The Wacker Ingot Casting Process, Materials Processing—Theory and Practices, Vol. 6, Silicon Processing for Photovoltaics II, North-Holland, Amsterdam, 1987, p. 97.
[6] Progress Report ACCESS e.V. 1996, unpublished.
[7] I. Steinbach, H.-U. Höfs, Microstructural analysis of the crystallization of silicon ribbons produced by the RGS process, Proceedings of the 26th Conference on Photovoltaic Solar Energy Conversion, Anaheim, 1997, p. 91.